Chapter 7

Sub-Pilot-Scale Hybrid Electrochemical System for Water Treatment and Hydrogen Production using a solar PV panel

Abstract

There is a clear need for environmentally-friendly alternative energy sources (without carbon emissions) and photovoltaic/electrolysis for hydrogen production via water splitting using organic contaminants as sacrificial electron donors can be a potential solution. This chapter demonstrates the feasibility of a sub-pilot scaled rooftop hybrid photovoltaic-electrolysis system for wastewater treatment with simultaneous hydrogen production. Application of an anodic bias of > 2.0 V to bismuth-doped TiO_2 (BiO_x-TiO_2)/Ti metal electrode results in the electrochemical degradation of a variety of organic contaminants (i.e., rhodamine B (Rh.B), methylene blue (MB), salicylic acid, triclosan, and phenol) and real wastewater from chemical industry, while molecular hydrogen is released at the counter stainless steel (SS) electrode. The kinetics of anodic substrates oxidation is investigated as a function of the cell current (I_{cell}), substrate concentration, and background electrolytes such as NaCl and Na_2SO_4, and average current efficiencies are shown in the range of 4–22 %. Cathodic current efficiency and energy efficiency for hydrogen production was achieved at 50–70% and 20–40%, respectively.

Introduction

In recent years, there has been increasing interest in an developing electrochemical method for wastewater treatment because of its advantages, including versatility, energy efficiency, amenability to automation, and robustness [1-3]. This technology was first tested with various synthetic wastewaters containing specific target compounds such as dyes and phenol [4-7], and more recently has focused on the treatment of actual wastewaters, including domestic wastewater, industrial wastewater, and landfill leachate [8-10]. However, the main drawback of electrochemical wastewater treatment is its high operating cost due to high electric energy consumption.

Hydrogen is considered as a possible alternative energy resource [11]. However, most hydrogen is produced by the well-established thermal process known as steam methane reforming (SMR), which has both supply issues and significant carbon emissions. Therefore, transition to a hydrogen economy may be considered when alternative renewable technologies to replace fossil-based hydrogen production methods are developed. In this context, electrolytic production of hydrogen (i.e., water electrolysis) is a potential solution to produce large amounts of hydrogen without the carbon emission associated with fossil fuel. However, the primary disadvantage of water electrolysis is also the high electric consumption, especially in large-scale application.

Over the past decades, electrochemical applications for water splitting and for wastewater treatment have been independently studied. A dual-purpose hybrid electrolysis system that couples wastewater treatment with hydrogen generation may make the electrolysis system economically feasible. In a hybrid system, electrochemical oxidation of organic contaminants takes place at an anode while a reduction reaction

simultaneously takes place at the cathode, resulting in hydrogen production. In previous studies, our group successfully demonstrated a hybrid electrochemical cell consisting of BiO_x–TiO_2/Ti(0) anodes and stainless steel (SS) cathodes for the complete oxidation of phenol with simultaneous hydrogen production [12-14].

In this study, we scaled up the hybrid electrolysis system to a sub-pilot size (a volume of 20 L) with BiO_x–TiO_2/Ti(0) anodes and SS cathodes to investigate the feasibility of a practical application. The kinetics of oxidative degradation of a variety of target substrates such as methylene blue (MB), rhodamine B (Rh.B), phenol, salicylic acid, triclosan, and waste organics in real industrial wastewater are investigated with simultaneous hydrogen production. In addition, a solar-driven rooftop hybrid electrolysis system using a commercial photovoltaic (PV) array is also investigated.

Experimental

Electrode Preparation

BiO_x–TiO_2/Ti(0) electrode was used as an anode and stainless steel (SS, Hastelloy C-22) was used as a cathode. The anode consists of a series of metal oxide coatings on a titanium metal plate: (a) a Ti metal substrate, (b) an anti-passivation layer (pre-coat) having the mixture of IrO_2 and Ta_2O_5, (c) an intermediated layer (seal coat) of SnO_2 and Bi_2O_3, (d) a slurry coat containing particles of TiO_2 doped with Bismuth (Bi), and (e) the overcoat with TiO_2 and Bi_2O_3. Slurry coat and overcoat together form the electrocatalytic outer layer of the electrode and each coating step requires a specific heat treatment at different temperatures and durations. This electrode exhibits excellent stability and long service life [15]. More details on the anode preparation are provided elsewhere [14,15]. Each

electrode plate is about 800 cm^2 and a reactor consists of 5 anodes and 6 cathodes that face each other with an interelectrode gap of 2 mm. (Figure 7.1)

Electrolysis Experiments

Electrolysis experiments were carried out in a sub-pilot scaled reactor with a volume of 20 L. Schematic diagram of the overall hybrid electrolysis is shown in Figure 7.1. The electrode couple (5 BiO_x–TiO_2/Ti(0) anodes and 6 SS cathodes) was immersed in 20 L of tap water. NaCl (J.T.Baker) was used as a primary supporting electrolyte in the range of 0–75 mM (typically 50 mM) and Na_2SO_4 (EMD) was also used to compare electrolyte effect to NaCl. Seawater, which was collected from a beach area near Los Angeles, CA, was used as a source of electrolyte as well. For the electrochemical oxidation, the target substrates such as Methylene Blue (MB, J.T.Baker), Rhodamine B (Rh.B, Aldrich), salicylic acid (SA, Aldrich), phenol (PhOH, Mallinckrodt), and 5-chloro-2-(2,4-dichlorophenoxy)phenol (triclosan, Fluka) were added in a background electrolyte solution and the solution was continuously circulated by the pump connected to the bottom of a reactor. Most experiments were performed at circumneutral pH except the experiment of triclosan at pH 12 adjusted with NaOH (EM Science) because of its very low solubility in neutral pH. Electrochemical degradation of highly contaminated chemical industry wastewater, which was sampled from the wastewater stream of a manufacturing facility located in Minnesota, was also investigated. Original wastewater was diluted with tap water to a proper COD concentration for laboratory experiments (150–300 ppm). A constant current in a range between 7.5 A and 40 A (typically 25 A) or voltage (3–4 V) was applied to the electrode couples by a DC power supply (HP

6260B), and cell voltage (E_{cell}) and cell current (I_{cell}) were measured during electrolysis by multimeters (Fluke).

Solar-Driven Electrolysis Experiment

For solar-driven electrolysis, a commercial polycrystalline silicon solar photovoltaic (PV) panel (Silicon Solar, Inc.) with a peak power output of 180 W (E_{peak} = 25.9 V and I_{peak} = 6.95 A, respectively) and with surface area of 1.50 m^2 (dimensions: 0.95 m × 1.57 m) was installed on the roof of the W. M. Keck Laboratories in Pasadena, CA. The solar PV panel was directly connected to a sub-pilot reactor to drive various electrochemical reactions such as the oxidative degradation of various organic contaminants and wastewater with simultaneous hydrogen production. Aqueous solutions of 50 mM NaCl and 2L (10 v/v %) of seawater were used as the primary electrolytes in the rooftop experiments. In addition to measurement of E_{cell} and I_{cell}, a real-time solar radiation was also monitored by a pyranometer (Apogee) with a datalogger (Campbell Scientific).

Analytical Methods

Sample aliquots were withdrawn from the solution intermittently during the electrolysis and analyzed. The color removal of dyes was monitored by measuring the absorbance at 665 nm and 550 nm for MB and Rh.B, respectively, with a UV/Vis spectrophotometer. The degradation of phenol, salicylic acid, and triclosan were monitored using a HPLC (Agilent 1100 series) equipped with a C18 column and a UV detector. The mobile phase was composed of 45 % acetonitrile and 55 % Milli-Q water containing 0.1 wt % acetic acid. For real wastewater, the chemical oxygen demand

(COD) was measured titrimetrically with COD reagent vials (Hach), which use dichromate as the oxidant in acidic solution at 150 ^{o}C for 2 hrs. $AgNO_3$ (Aldrich) was added into sample solution before measuring COD to eliminate the chloride interference in cases where NaCl was used as an electrolyte. In addition, COD removal of other substrates was also measured to determine the current efficiencies for the anodic oxidations.

Molecular hydrogen (H_2) produced from water during electrolysis was detected by a quadruple mass spectrometry (MS, Balzers). As shown in Figure 7.1, the reactor was sealed and the headspace gas of the reactor was extracted with a peristaltic pump and pushed into a quadruple MS with 70 eV electron ionization energy via a turbo pump (Pfeiffer; 5.0×10^{-6} Torr). The production rate of H_2 was calculated from the volume percent of H_2 in the headspace gas, which was measured assuming that it was directly proportional to the percent of ion current of H_2 in total ion currents measured by MS.

Current Efficiency and Energy Efficiency

The instantaneous current efficiencies (ICE) for anodic oxidations were calculated using the following equation introduced by Comninellis and Pulgarin [6,16]:

$$ICE\ (\%) = \frac{[COD_0 - COD_t]FV}{8It} \times\ 100$$

where COD_0 and COD_t are the COD (in g O_2/L) before and after electrolysis, respectively, F is the Faraday constant (96,487 C/mol), V is volume of the electrolyte (in L), I is the current (in A), and t is a reaction time (in s).

Since the ICE decreases with time during electrolysis to finally reach about zero, the electrochemical oxidation index (EOI), which expresses the average current efficiency, was also calculated from following equation:

$$EOI(\%) = \frac{\int ICE}{\tau}$$

where τ is the time of electrolysis at which ICE is almost zero.

For H_2 production, the cathodic current efficiencies (CE) were calculated by the following:

$$CE\ (\%)\ for\ H_2\ = \frac{2 \times\ numbers\ of\ H_2\ molecules\ produced}{numbers\ of\ electron\ flew} \times\ 100$$

Energy efficiencies (EE) for H_2 production use the higher heating value of H_2 (HHV, 39 Wh/g) and the energy consumed by the system:

$$EE\ (\%)\ for\ H_2\ = \frac{39\ Wh/g\ \times\ H_2\ prod.rate\ (mol/h)}{E_{cell}\ (V) \times\ I_{cell}(A)} \times\ 100$$

In solar-powered electrolysis system, the energy efficiencies were calculated by the following equations:

$$solar\ to\ PV_{cell}\ \ EE\ (\%) = \frac{E_{cell}\ (V)\ \times\ I_{cell}(A)}{solar\ flux\ (W/m^2)\ \times\ PV\ area\ (m^2)} \times\ 100$$

$$solar\ to\ H_2\ \ EE\ (\%) = \frac{H_2\ EE\ (\%)\ \times\ solar\ to\ PV_{cell}\ \ EE\ (\%)}{100}$$

Results and Discussion

Electrochemical Water Treatment

Figure 7.2(a) shows a typical E_{cell}–I_{cell} curve at the BiO_x–TiO_2/Ti(0) anode coupled with stainless steel cathode in a sub-pilot reactor in presence of sodium chloride or

sodium sulfate as a supporting electrolyte. The current is generated around 2.0 V of applied voltage linearly increased above 2.5 V of E_{cell}. The use of Na_2SO_4 as a supporting electrolyte generates higher current density than NaCl at the same applied voltage. We also measured E_{cell}–I_{cell} curve in the presence of 10 v/v% seawater, which was sampled from a beach area near Los Angeles, CA, instead of adding NaCl (since seawater typically contains 0.5 M NaCl) and observed that current density in the presence of 10 v/v % seawater was slightly higher than that in 50 mM NaCl, which may be because of other salts present in seawater; conductivity of solution adding 10 v/v % of seawater was measured at 5.3–5.6 mS/cm. Figure 7.2(b) shows the current density as a function of the concentration of electrolytes at 3 V of applied voltage. The current density increases with the addition of electrolyte, but it does not increase much at high concentration of electrolyte (i.e., more than 50 mM). Therefore, the concentration of electrolytes was fixed at 50 mM (or 10 v/v % seawater) in the following experiments.

Figure 7.3 shows the effect of applied current density on the electrochemical degradation of organic substrates using NaCl or Na_2SO_4 as supporting electrolytes in a sub-pilot reactor. Figure 7.3(a) shows the electrochemical degradation (i.e., color removal) of MB at different applied cell current in the presence of NaCl. As expected, increasing the current density resulted in a faster decolorization of MB due to a greater charge entering the cell and more electro-generating of oxidants such as $OH^{\cdot}$ radicals and active chlorine species. The decolorization follows first-order kinetics and the apparent degradation rate constant of MB (k_{MB}) was proportional to the current density (Figure 7.3a, inset). Figure 7.3(b) also shows that the degradation rate constant of triclosan (k_{TCS}) is increased as higher current density is applied in the presence of 50 mM Na_2SO_4.

The effect of type and concentration of electrolytes on MB degradation is investigated in Figure 7.4. Figure 7.4(a) shows that MB degradation in the presence of NaCl was much faster than Na_2SO_4 although current density in the presence of NaCl was relatively lower than that in the presence of Na_2SO_4 (Figure 7.2). The same tendency was observed in the degradation of other organic substrates, such as Rhodamine B (Rh.B) and salicylic acid (S.A.), as shown in Table 7.1. In the presence of 50 mM NaCl, half-life time ($t_{1/2}$) for the degradation of Rh.B and S.A. was estimated less than 2 min each, whereas it was remarkably increased to 27 min and 77 min, respectively, in the presence of Na_2SO_4. It has been frequently reported that NaCl enhances the electrochemical degradation efficiency for various organic substrates (e.g., MB, phenol, glucose, and 17 β–estradiol) as compared to Na_2SO_4 [4,6,17,18]. The electrochemical degradation of organic substrates can occur via direct oxidation on the anode surface (eq.7.1), indirect oxidation mediated by $OH^{\cdot}$ radicals (eq.7.2), and indirect oxidation mediated by electro-generated oxidant from electrolyte solution such as $Cl^{\cdot}$, $Cl_2^{\cdot -}$, and OCl^- in the presence of NaCl (eqs.7.3–7.7):

$$\text{org.} \rightarrow \text{oxidized org.} + e^- \quad (7.1)$$

$$H_2O \rightarrow OH^{\cdot} + H^+ + e^- \quad (7.2)$$

$$Cl^- \rightarrow Cl^{\cdot} + e^- \quad (7.3)$$

$$Cl^- + Cl^{\cdot} \rightarrow Cl_2^{\cdot -} \quad (7.4)$$

$$Cl_2^{\cdot -} + H_2O \rightarrow HOCl + Cl^- + H^+ + e^- \quad (7.5)$$

$$Cl_2^{\cdot -} + OH^{\cdot} \rightarrow HOCl + Cl^- \quad (7.6)$$

$$HOCl \leftrightarrow OCl^- + H^+ \quad (pKa = 7.46) \quad (7.7)$$

In the presence of NaCl electrolyte, active chlorine species such as $Cl^{\cdot}$, $Cl_2^{\cdot -}$, and OCl^{-}, which are electrochemically generated at the anode surface, act as powerful oxidants during electrolysis, resulting in fast substrates oxidation when compared to the use of other electrolytes. In our previous study, $Cl_2^{\cdot -}$ was assumed the primary oxidant among various active chlorine species since the observed degradation rates are found to be proportional only to the bimolecular rate constants of $Cl_2^{\cdot -}$ with the substrate [13]. On the other hand, indirect oxidation by $OH^{\cdot}$ radicals and $SO_4^{\cdot -}$ radicals (eq.7.8) can take place in Na_2SO_4 solution as well. However, substrates oxidation rates with Na_2SO_4 are observed very low, implying that a lower concentration of $OH^{\cdot}$ radicals are produced in Na_2SO_4 solution and(or) $SO_4^{\cdot -}$ radicals are less determining of the reaction rates, in spite of their high redox potential. It is ascribed to the generation of surface-bound $SO_4^{\cdot -}$ radicals at metal oxide electrode surface and reaction with another $SO_4^{\cdot -}$ to produce persulfate (eq.7.9):

$$SO_4^{2-} \rightarrow SO_4^{\cdot -} + e^{-} \quad (7.8)$$

$$SO_4^{\cdot -} + SO_4^{\cdot -} \rightarrow S_2O_8^{2-} \quad (7.9)$$

A substrate oxidation rate with 10 v/v % of seawater was even higher than that with 50 mM NaCl, suggesting that the seawater could be a good alternative source of NaCl electrolyte, as shown in Figure 7.4(a). Figure 7.4(b) shows the effect of the concentration of NaCl (SW) electrolyte on MB degradation rates. In the absence of NaCl electrolyte, MB was degraded very slowly ($k_{MB} \sim 1.8 \times 10^{-2}$ min^{-1}) while MB degradation rates increased by an order of magnitude (k_{MB}= 1.1–3.9 $\times 10^{-1}$ min^{-1}) as NaCl was added. However, degradation rates do not increase at higher concentration, which is similar to the change of current density as a function of the concentration of electrolyte (Figure

7.2b). Inset of Figure 7.4(b) shows a linear relationship of the degradation rates and current densities generated by adding different concentration of electrolytes, suggesting that electrolyte concentration can affect the degradation rates by a change of current density.

Table 7.1 summarizes the degradation rate constants of several organic substrates under various conditions. The initial concentration had no significant effect on MB degradation rate. For example, k_{MB} at $[MB]_0$= 5 μM was faster than those at higher concentration of MB, however, k_{MB} does not decrease further over the range of 10–250 μM (see Figure 7.5(a), inset, also). The half-life time ($t_{1/2}$) for MB degradation at $[MB]_0$= 10 μM and 250 μM was estimated at 5 min and 7 min, respectively. However, the initial concentration of phenol significantly affects the apparent degradation rate of phenol. For example, k_{PhOH} decreased remarkably at higher concentration, which is due to production of a large number of reaction intermediates such as chlorinated phenols. Figure 7.5 also compares COD removal with the substrate removal of MB and phenol. For MB degradation, as expected, COD removal rate was slower than color removal rate, suggesting that MB was oxidized first to colorless intermediates and then oxidized further to CO_2. However, k_{COD} was almost similar to k_{osb} at $[MB]_0$= 10 μM and 2 times higher than k_{obs} at $[MB]_0$= 100 μM (Table 7.1). For phenol degradation, however, substrate degradation was completed within 2 min, but COD reduction was continued for more than 10 min (i.e., $k_{COD} >> k_{obs}$ in Figure 7.5b). It implies that the COD reduction and full oxidation step of MB is simpler and(or) intermediates do not significantly interfere with parent MB molecules as compared to the process of COD reduction and mineralization of phenol.

The current efficiencies (i.e., ICE) of anodic substrate oxidations determined from COD measurement are shown in Figure 7.6. The current efficiency was higher at the initial stages (e.g., 85 % for MB oxidation) and decreased with time during electrolysis (Figure 7.6a). Current efficiency also depends on the type of substrates and applied current density. Low initial concentration results in higher current efficiencies. For example, low initial concentration of MB showed higher current efficiency than high initial concentration. In addition, current efficiency increases also with low applied current density whereas the substrate removal efficiency increases with high current density. The current efficiency of phenol at applied I_{cell} of 8 A was higher than that with 25 A applied. Figure 7.6(b) compares the average current efficiencies (i.e., EOI) for various substrates oxidation. The average current efficiencies were in the range of 10–20 % with the order of MB > Rh.B > phenol at the same initial concentration.

Figure 7.7 shows the electrochemical oxidation of real wastewater from chemical industry. COD decreased during electrolysis and the removal efficiency increased at high applied voltage. The average current efficiency was determined to be about 4%. It is relatively lower than current efficiencies (10–20 %) for the oxidation of a specific substrate, indicating that the real wastewater likely contain more persistent organic substrates and(or) other unknown species present in wastewater may compete to desirable substrate oxidation, resulting in low current efficiency.

In conclusion, our sub-pilot electrochemical system is proven for complete oxidation and mineralization of a variety of environmental organic pollutants and real wastewater. NaCl is the most effective electrolyte for fast wastewater treatment in our system, which can be replaced by seawater.

Simultaneous H_2 Production via Water Electrolysis

A significant amount of H_2 is simultaneously produced from water electrolysis at the cathode in a sub-pilot hybrid electrochemical reactor under various conditions (Table 7.2). For pure water splitting in the absence of organic substrates, H_2 production rates are in the range of 3–5 L/hr and current efficiencies (CE) and energy efficiencies (EE) are about 50–60% and 20–35%, respectively. As expected, a sub-pilot reactor showed lower efficiency than a small size reactor with 35–60% of EE. The current efficiency and energy efficiency for H_2 production also decreased with increasing applied power, which showed the same tendency as substrates oxidation at the anode. In addition, we compared Na_2SO_4 with NaCl and observed that Na_2SO_4 was better than NaCl for the H_2 production efficiency. It may be due to high current densities generated in Na_2SO_4 solution as compared to the same concentration of NaCl (Figure 7.2) and no electron relay between the anode and the cathode via chlorine species. In NaCl solution, active chlorine species produced at anode can be reduced again at the cathode and fewer electrons are available for H_2 production at cathode. When 10 v/v % of seawater was used as an electrolyte source, H_2 production rate is higher than in50 mM NaCl.

In the presence of organic substrates such as MB and phenol, H_2 production rates measured at 5–6 L/hr of with simultaneous oxidation of substrates. H_2 production rates remained almost constant before and after adding organic substrates. In addition, a similar H_2 production rate was obtained with industrial wastewater as well, suggesting that the presence of waste organics in solution does not have a negative effect on cathodic H_2 production. In previous studies, we have suggested that some organic substrates can actually increase H_2 production energy efficiencies by 30–50% in a NaCl electrolyte

system by quenching active chlorine species, which compete with H_2 production reactions for cathodic electrons [13,14]. Active chlorine species can act as an electron shuttle by being oxidized at the anode and reduced at the cathode. If organic substrates are added, however, substrates are rapidly oxidized by active chlorine species and this electron relay can be consequently inhibited, resulting in increasing H_2 production rates by making more electrons available at the cathode. However, this synergic effect on H_2 production was not observed with industrial wastewater treatment in a sub-pilot electrolysis system, which may be because a synergic effect is dependent on the type of organic substrates [13]. It may also be due to relatively low production rates of active chlorine species as compared with H_2 production rates in a sub-pilot system. For example, we compared H_2 production rate with hypochlorite (OCl^-) production rate, which is one of the active chlorine species and easily detected using UV/vis spectrometer. In a small size of electrochemical reactor, H_2 production rate of 100–300 μM/min was comparable to OCl^- production rate of 100–150 μM/min, which can result in big inhibition effect of active chlorine species on the H_2 production reactor. In a sub-pilot reaction, however, H_2 production rate significantly increased to 3–5 mM/min whereas OCl- production rate was still remained similar (200 μM/min).

Solar-Driven Hybrid Electrolysis System

Figure 7.8 shows the results of solar-driven photovoltaic-electrolysis experiments with our sub-pilot hybrid reactor, which was performed on the rooftop of W. M. Keck Laboratories at Caltech in August 2009. We directly connected 180 W_{peak}-rated commercial PV panel with surface area of 1.50 m^2 to BiO_x–TiO_2/Ti(0) anode and SS

cathode. Figure 7.8(a) shows typical time profiles of solar light radiation energy measured by a pyranometer, E_{cell}, and I_{cell} on sunny day. The peak of solar radiation energy was measured about 1000 W/m^2 around 12:30 PM and decreased to 600 W/m^2 in the late afternoon. E_{cell} measured 3.3 V in the presence of 10 v/v % seawater as an electrolyte and slightly decreased to 3.0 V in the afternoon as solar irradiation energy decreased while I_{cell} was measured about 7 A both in the morning and in late afternoon. Solar irradiation energy, E_{cell} and I_{cell} was measured for several days including a partly cloudy day on August, 2009 and remained approximately constant with E_{cell} of 2.7–3.3 V and I_{cell} of 6–7 A. The actual PV output power was measured 23 W, which is only 13 % of PV_{peak} output power reported by supplier, possibly due to losses from wiring, heat, and coupling to the electrolyzer. Solar-to-PV_{cell} energy efficiency was determined to be 1.6–2.0 %, whereas it was about 2.5 % with a system consisting of a 6.4 W_{peak}–rated small PV panel (the area of 0.13 m^2) and a small electrolyzer (200 mL).

MB and industrial wastewater were effectively treated in spite of low output power, as shown in Figure 7.8(b). For example, the apparent kinetic constant for COD reduction (k_{COD}) of 3M wastewater with solar-driven system by PV array operating at 21 W ($E_{cell} \times I_{cell}$ = 3.0 V × 7 A) was estimated to be 9.0×10^{-3} min^{-1}, which is a similar k_{COD} to DC-powered oxidation operated at 45 W ($E_{cell} \times I_{cell}$ = 3.0 V × 15 A). The average current efficiency for industrial wastewater oxidation was increased to 15% in solar-driven system, which is almost 4 times higher than that with DC-powered oxidation. This high efficiency may be because the photo-assisted electrochemical (i.e., photoelectrochemical, PEC) reactions took place in solar-powered rooftop experiment. A sub-pilot electrolyzer was installed on the roof as well to connect directly to the PV panel, and therefore some

of the solar-light could pass through the reactor and the PEC processes could be initiated by doped TiO_2 particles coated on an anode surface. Preliminary results of laboratory experiment with a medium size of electrochemical reactor and using the artificial UV lamp shows that the electrochemical oxidation rates of phenol were increased with UV light irradiation, indicating that the PEC processes actually take place on BiO_x–TiO_2/Ti(0).

In solar-driven hybrid electrolysis system, it was also observed that sufficient amount of H_2 was continuously produced with simultaneous oxidation of waste organic substrates. H_2 production rate was measured at 2.2 L/hr, which was smaller than that of the DC-powered system (Table 7.2). In spite of relatively low power, however, CE and EE were increased to 74 % and 38 %, respectively. Like anodic oxidation, high CE and EE for H_2 production in solar-driven electrolysis system can be ascribed to photocatalytic activity of TiO_2 on anode surface. In DC-powered electrolysis with a medium size of electrolyzer, we also found that photoelectrochemical (PEC) H_2 production rates under UV light irradiation were almost 2 times higher than electrochemical H_2 production rates in the absence of UV light. Solar-to-H_2 energy efficiency was determined 0.8 %.

Practical Application

The above results show an example of a sub-pilot hybrid photovoltaic-electrolysis system, which has dual purposes for both wastewater treatment and H_2 production. In the solar-driven experiment, solar-to-H_2 energy efficiency was estimated less than 1 %, which was lower than other commercial PV-electrolysis systems in the range of 2–10 % [19-22]. However, it is difficult to compare our hybrid PV-electrolysis system with other

commercial PV-electrolysis systems since ours has several distinguishable advantages for practical application. First, our hybrid PV-electrolysis system can be operated at mild conditions, whereas other types of PV-electrolysis systems can be only operated at much harsher conditions. For example, the alkaline water electrolyzer, the most commercialized electrolyzer, uses an extremely high concentration of alkaline electrolytes (i.e., 6–7 M KOH) resulting in high pH environment which is also operated at about 70–80 ^{o}C in general and under pressure is desirable to minimize energy requirement [23]. However, our hybrid PV-electrolysis system can be effectively operated at circum-neutral pH condition and relatively low concentration of electrolyte (e.g., 50 mM NaCl). Second, our PV-electrolysis system has dual purposes for real wastewater treatment and H_2 production, which can make this technology economically feasible. Other PV-electrolysis systems that previously reported generally use alkaline electrolyzer or PEM electrolyzer (a second commercially available electrolyzer), which is impractical for application to water treatment. On the other hand, our sub-pilot PV-electrolysis system is also working for various wastewater treatments, suggesting that electrochemical water treatment can be successfully implanted with water splitting into hydrogen.

The PV-electrolysis system employed in this study can be also distinguished from other electrochemical water treatment system in terms of using new types of anode material and PV array for power supply. For example, boron-doped diamond electrode (BOD) is known as the most promising anode for wastewater treatment because of its high stability, wide potential window of water discharge, and a relatively low background current [24-26]. Jiang et al. also showed that the decomposition of waste organics and

simultaneous hydrogen production are feasible with a boron-doped diamond (BOD) electrode [24]. However, pilot scale application would be limited with BOD electrode due to its high price and size limitation since the production typically involves chemical vapor deposition (CVD) or high pressure-high temperature (HPHT) processes [27]. On the other hand, the Bi-doped TiO_2 anode employed in this study had been easily manufactured in a pilot scale with relatively low cost [15]. In addition, a PV-electrolysis system for environmental applications (i.e., water treatment) was proposed to reduce the operating cost– in a way not demonstrated before to our knowledge [24]. In this study, we demonstrated a sub-pilot PV-electrolysis system for water treatment and also showed a synergic effect on water treatment as compared to DC-powered system, since photoelectrochemical processes can be possible with Bi-doped TiO_2 anodes when a photovoltaic system is combined.

Figure 7.1. Schematic diagram of a sub-pilot electrochemical reactor and overall hybrid system

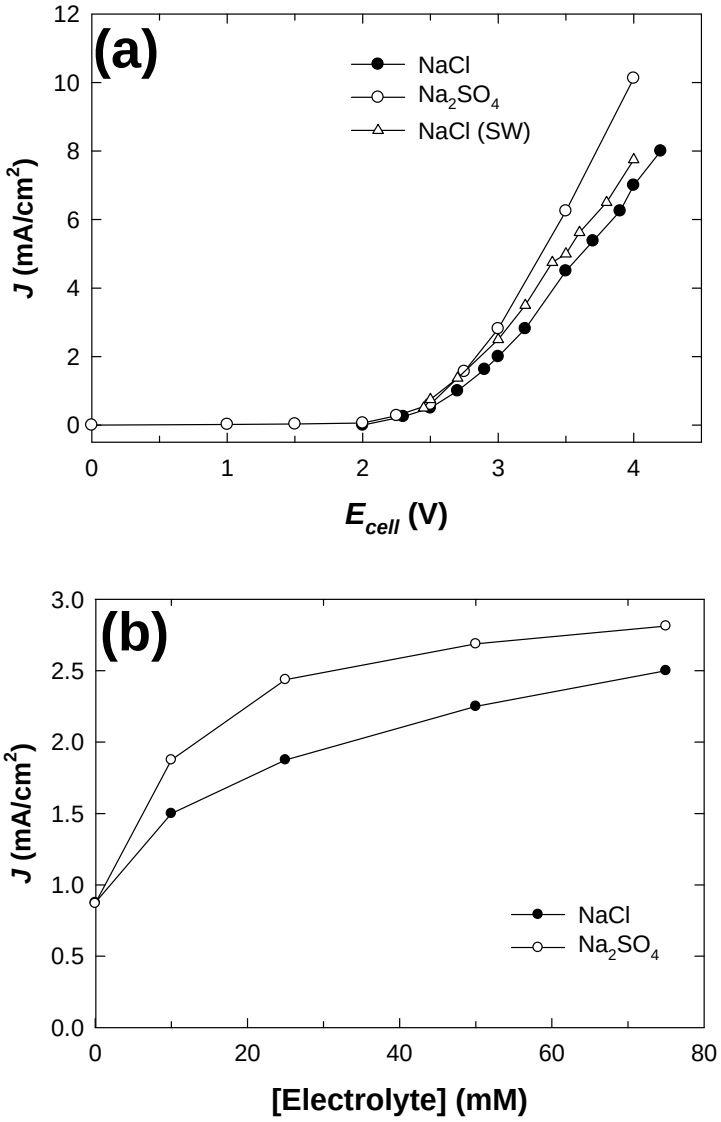

Figure 7.2. (a) E_{cell}–I_{cell} plot in the presence of 50 mM NaCl or Na_2SO_4 as a supporting electrolyte. NaCl (SW) indicates 10 v/v % of seawater as a source of NaCl electrolyte. (b) The current density (J_{cell}) as a function of the concentration of the electrolyte (mM) at applied E_{cell} = 3.0 V

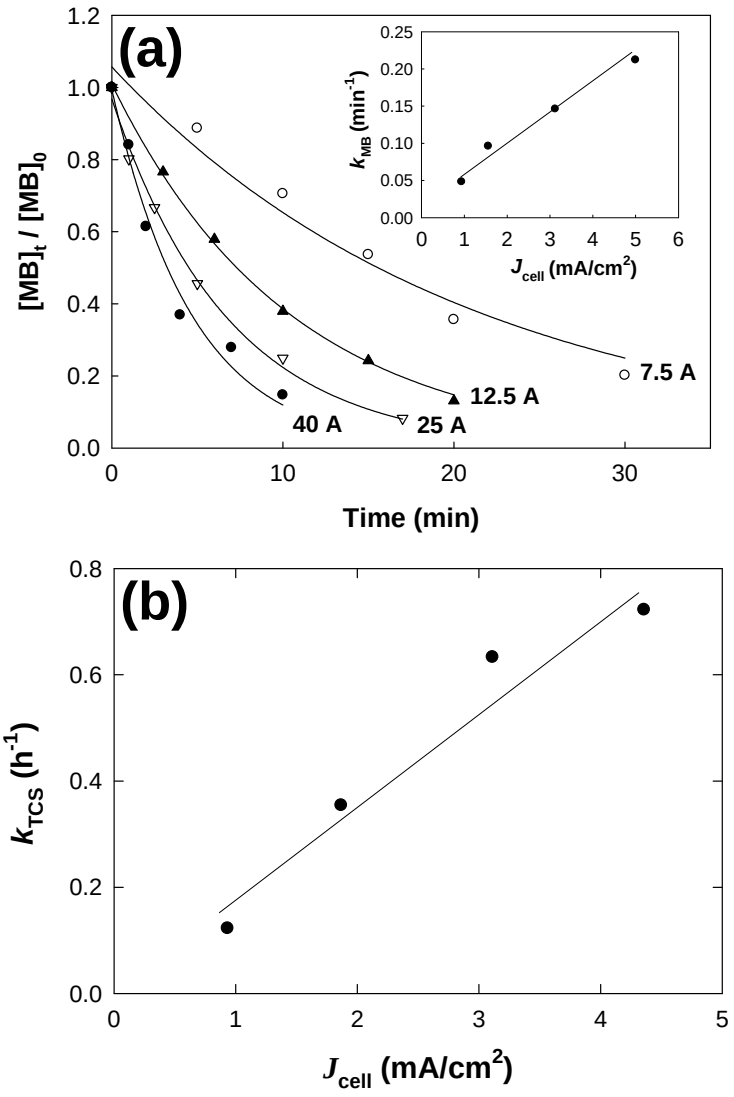

Figure 7.3. Electrochemical degradation of organic substrates as a function of applied current density: (a) The degradation of methylene blue ($[MB]_0$= 10 μM) in 50 mM NaCl, (b) the degradation of triclosan ($[TCS]_0$= 100 μM) in 50 mM Na_2SO_4.

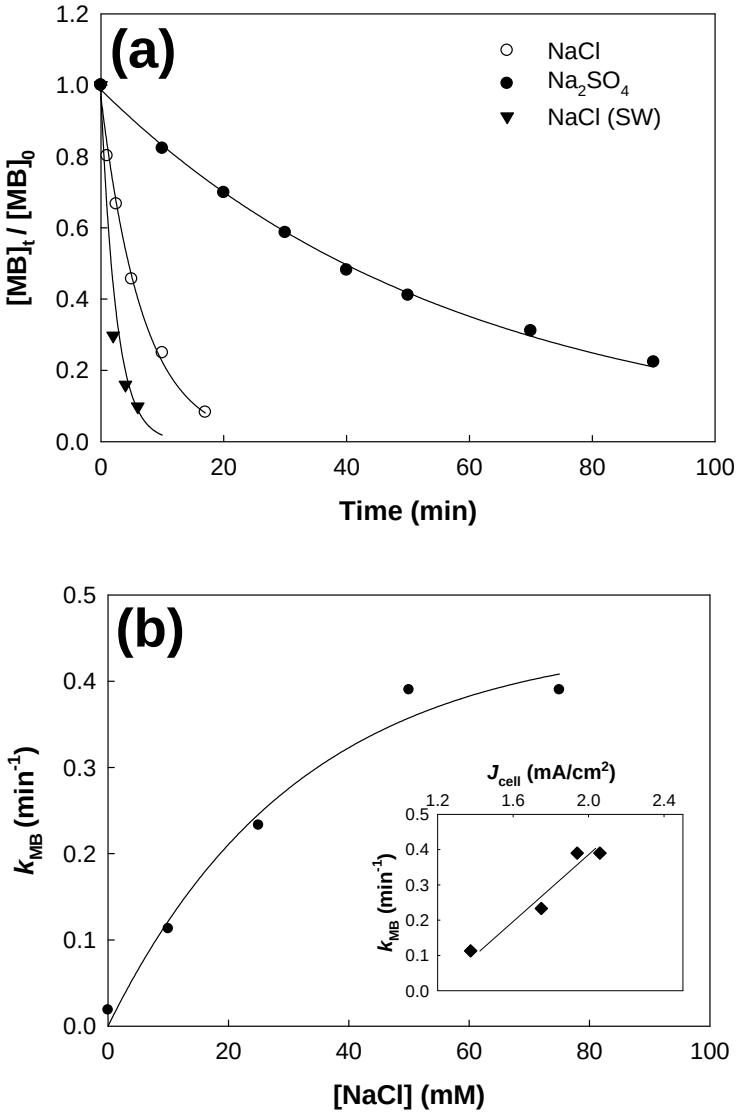

Figure 7.4. (a) Electrochemical degradation of methylene blue (MB) in the presence of different types of electrolyte at I_{cell}= 25A, $[MB]_0$= 10 μM. 50 mM NaCl, 50 mM Na_2SO_4, and 10 v/v % seawater (NaCl, SW) were used as background electrolytes. (b) The color removal rate constant of MB as a function of the concentration of NaCl (SW) electrolyte at E_{cell}= 3 V, $[MB]_0$= 10 μM.

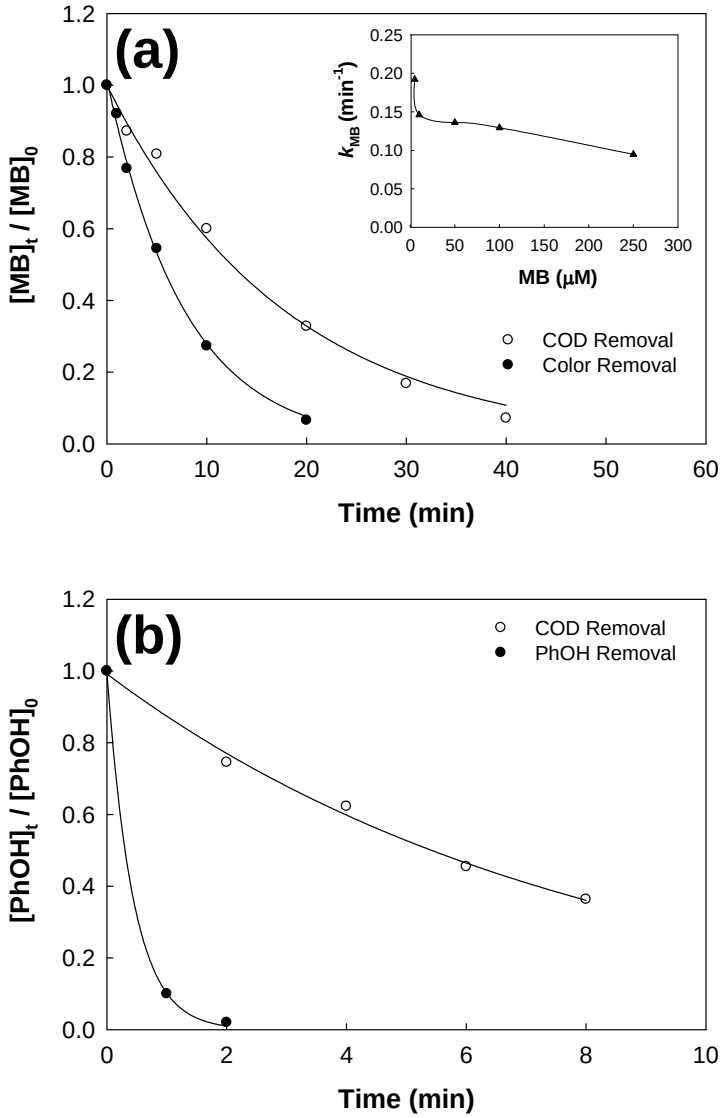

Figure 7.5. The electrochemical degradation of organic substrates vs. COD removal for (a) MB and (b) phenol at applied I_{cell}= 25A in the presence of 50 mM NaCl ($[MB]_0$= 10 or 100 μM, $[PhOH]_0$= 100 μM)

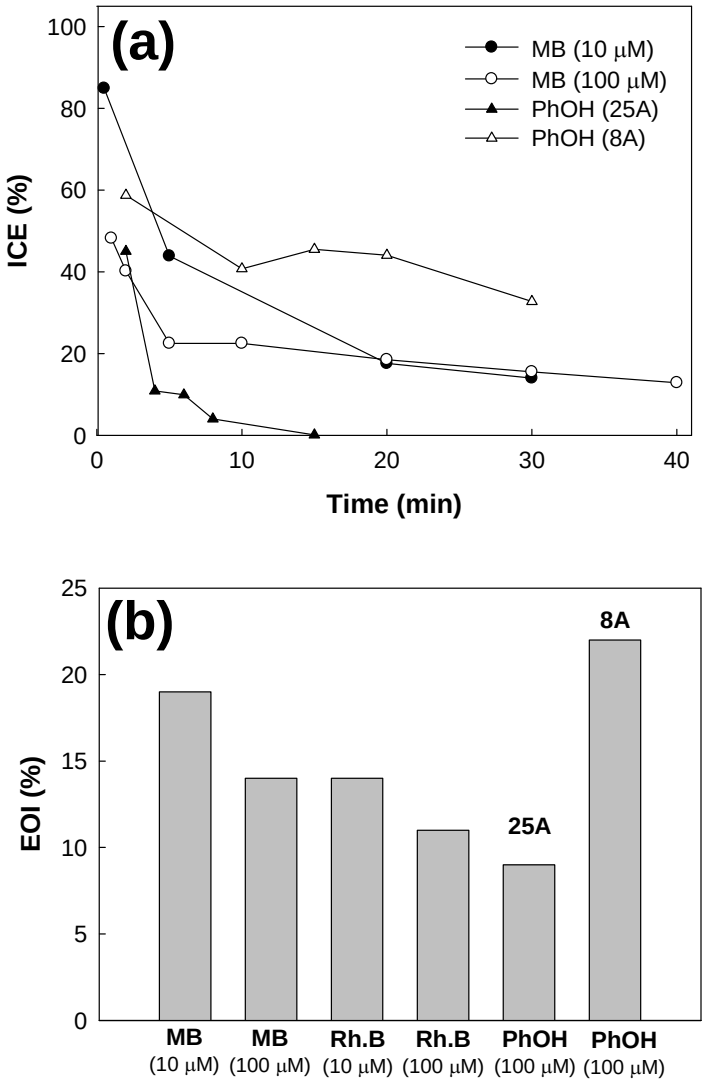

Figure 7.6. (a) Time profile of current efficiencies (ICE) and (b) average current efficiencies (EOI) for various substrates oxidations: $[MB]_0$= 10 or 100 μM, $[Rh.B]_0$= 10 or 100μM, $[PhOH]_0$= 100 μM, [NaCl(SW)]= 50 mM, I_{cell}= 25 A applied except PhOH(8A).

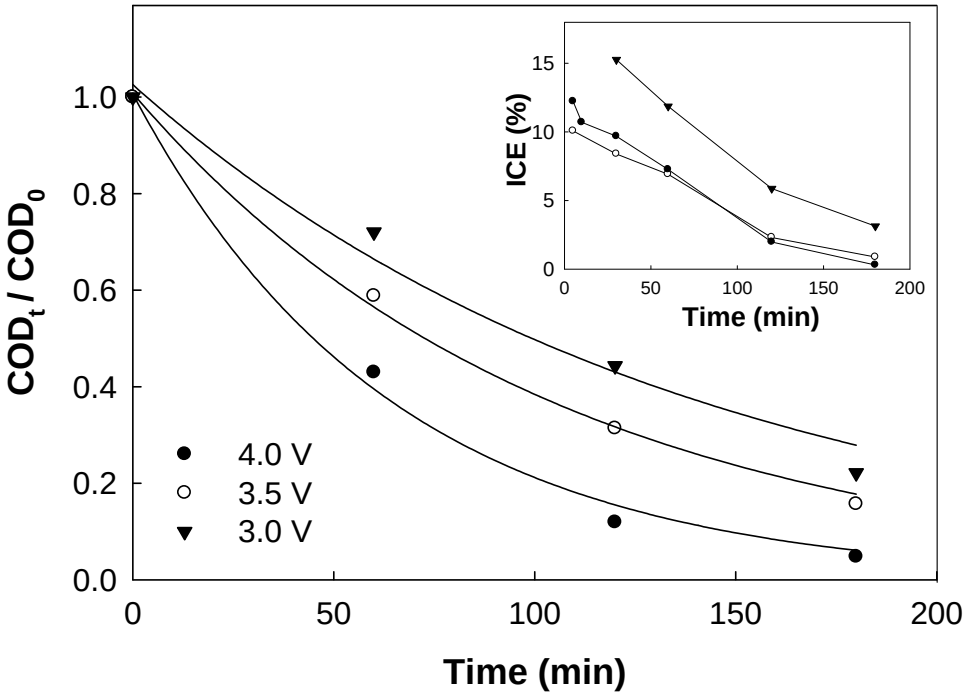

Figure 7.7. Electrochemical oxidation of industrial wastewater samples (COD_0= 100–150 ppm) at different applied voltages. 10 v/v % (2L) seawater was used as a source of NaCl electrolyte. Inset graph shows the current efficiencies and average current efficiency was determined about 4 %.

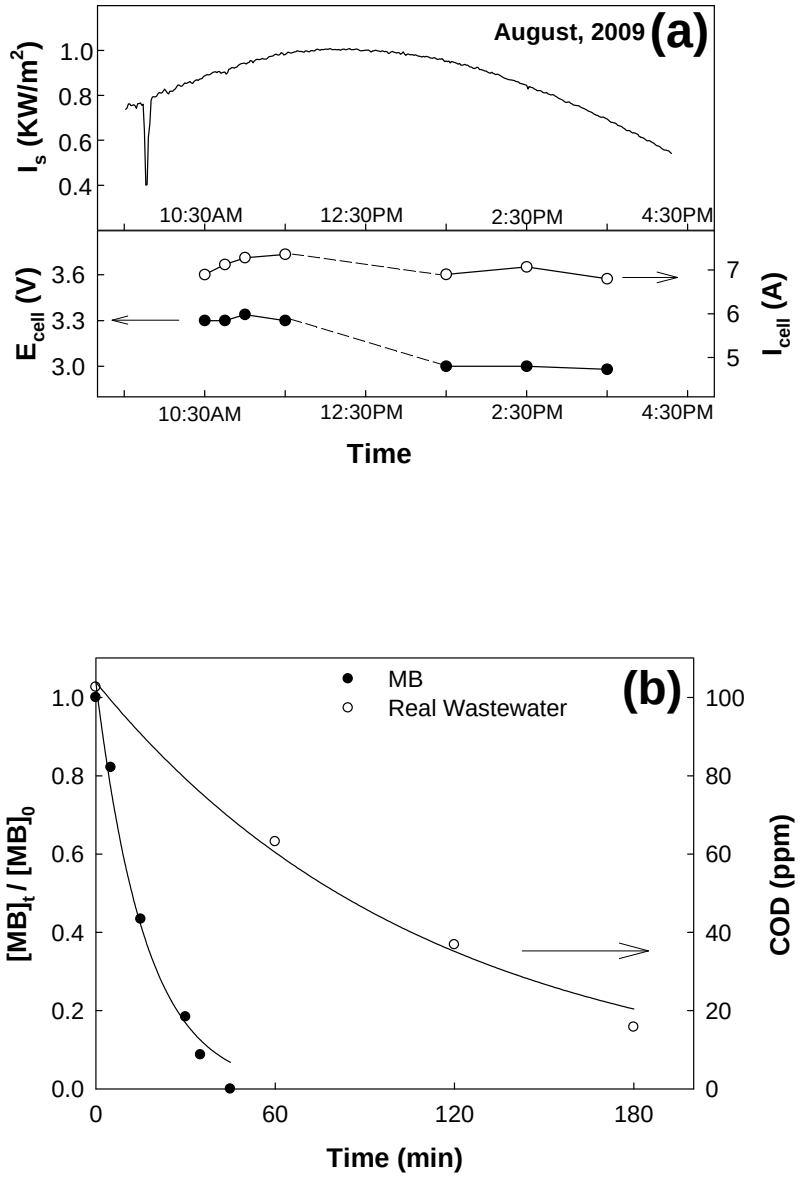

Figure 7.8. Solar-powered rooftop experiment: (a) solar intensity, cell current and cell voltage, which are measured during daytime. (b) The degradation of MB ($[MB]_0$= 100 μM) and COD removal of industrial wastewater (COD_0= 100 ppm). 10 v/v % (2L) seawater was used as an electrolyte in all experiments.

TABLE 7.1. The degradation rate constants for anodic oxidation of several organic substrates: 20 L sub-pilot reactor, I_{cell} = 25 A applied, [electrolyte]= 0.05M.

Substrate	**Conc. (µM)**	**Electrolyte**	k_{obs} **(min^{-1})**	$t_{1/2}$ **(min)**	k_{COD} **(min^{-1})**
MB	5	NaCl	0.192	3.6	
	10	NaCl	0.146	4.7	0.130
	50	NaCl	0.136	5.1	
	100	NaCl	0.129	5.4	0.056
	250	NaCl	0.095	7.3	
PhOH	100	NaCl	2.320	0.3	0.124
	250	NaCl	1.190	0.6	
	1000	NaCl	0.360	1.9	
Rh.B	100	NaCl	0.379	1.8	0.259
	100	Na_2SO_4	0.026	27	
S.A.	100	NaCl	0.420	1.7	
	100	Na_2SO_4	0.009	77	

TABLE 7.2. The rate, cathodic current efficiency (CE), and energy efficiency (EE) of hydrogen production: 20 L sub-pilot reactor, constant current applied, 0.05M of electrolyte used. (s.w. means 10 v/v % of seawater)

Substrate	Icell (A)	Ecell (V)	Electrolyte	H_2 prod. rate (L/hr)	CE (%)	EE (%)
water only	12.5	2.85	NaCl	3.2	60	31
	20	3.00	NaCl	4.0	48	23
	25	3.23	NaCl	4.3	42	19
	25	3.23	s.w.	5.0	48	21
	25	3.17	Na_2SO_4	5.2	50	23
MB	25	3.25	s.w.	5.3	51	23
PhOH	25	3.25	s.w.	5.7	55	25
wastewater	25	3.23	s.w.	5.0	48	22
wastewater (PV)	7	2.82	s.w.	2.2	74	38

References

(1) Juttner, K.; Galla, U.; Schmieder, H. *Electrochim. Acta* **2000**, *45*, 2575.

(2) Chen, G. H. *Sep. Purif. Technol.* **2004**, *38*, 11.

(3) Anglada, A.; Urtiaga, A.; Ortiz, I. *Journal of Chemical Technology & Biotechnology* **2009**, *DOI: 10.1002/jctb.2214*

(4) Panizza, M.; Barbucci, A.; Ricotti, R.; Cerisola, G. *Sep. Purif. Technol.* **2007**, *54*, 382.

(5) Shen, Z. M.; Yang, J.; Hu, X. F.; Lei, Y. M.; Ji, X. L.; Jia, J. P.; Wang, W. H. *Environ. Sci. Technol.* **2005**, *39*, 1819.

(6) Comninellis, C.; Nerini, A. *J. Appl. Electrochem.* **1995**, *25*, 23.

(7) Iniesta, J.; Michaud, P. A.; Panizza, M.; Cerisola, G.; Aldaz, A.; Comninellis, C. *Electrochim. Acta* **2001**, *46*, 3573.

(8) Vlyssides, A. G.; Karlis, P. K.; Rori, N.; Zorpas, A. A. *J. Hazard. Mater.* **2002**, *95*, 215.

(9) Vaghela, S. S.; Jethva, A. D.; Mehta, B. B.; Dave, S. P.; Adimurthy, S.; Ramachandraiah, G. *Environ. Sci. Technol.* **2005**, *39*, 2848.

(10) Urtiaga, A.; Rueda, A.; Anglada, A.; Ortiz, I. *J. Hazard. Mater.* **2009**, *166*, 1530.

(11) *International Energy Outlook 2006; DOE/EIA=0484(2008)*; Energy Information Administration, U.S. Department of Energy: Washington, DC, 2008.

(12) Park, H.; Vecitis, C. D.; Choi, W.; Weres, O.; Hoffmann, M. R. *J. Phys. Chem. C* **2008**, *112*, 885.

(13) Park, H.; Vecitis, C. D.; Hoffmann, M. R. *J. Phys. Chem. C* **2009**, *113*, 7935.

(14) Park, H.; Vecitis, C. D.; Hoffmann, M. R. *J. Phys. Chem. A* **2008**, *112*, 7616.

(15) Weres, O. Electrode with Surface comprising Oxides of Titanium and Bismuth and Water Purification Process Using This Electrode. In *United States Patent*, January 4, 2007.

(16) Comninellis, C.; Pulgarin, C. *J. Appl. Electrochem.* **1991**, *21*, 703.

(17) Murugananthan, M.; Yoshihara, S.; Rakuma, T.; Uehara, N.; Shirakashi, T. *Electrochim. Acta* **2007**, *52*, 3242.

(18) Bonfatti, F.; Ferro, S.; Lavezzo, F.; Malacarne, M.; Lodi, G.; De Battisti, A. *J. Electrochem. Soc.* **2000**, *147*, 592.

(19) Ahmad, G. E.; El Shenawy, E. T. *Renewable Energy* **2006**, *31*, 1043.

(20) Hollmuller, P.; Joubert, J. M.; Lachal, B.; Yvon, K. *Int. J. Hydrogen Energy* **2000**, *25*, 97.

(21) Lehman, P. A.; Chamberlin, C. E.; Pauletto, G.; Rocheleau, M. A. *Int. J. Hydrogen Energy* **1997**, *22*, 465.

(22) Gibson, T. L.; Kelly, N. A. *Int. J. Hydrogen Energy* **2008**, *33*, 5931.

(23) Srinivasan, S. *Fuel cells: from fundamentals to applications;* Springer: New York, 2006.

(24) Jiang, J. Y.; Chang, M.; Pan, P. *Environ. Sci. Technol.* **2008**, *42*, 3059.

(25) Cabeza, A.; Urtiaga, A. M.; Ortiz, I. *Ind. Eng. Chem. Res.* **2007**, *46*, 1439.

(26) Montanaro, D.; Petrucci, E.; Merli, C. "Anodic, cathodic and combined treatments for the electrochemical oxidation of an effluent from the flame retardant industry", 2008.

(27) Kraft, A. *Int. J. Electrochem. Sci.* **2007**, *2*, 355.